International Journal of Engineering & Technology
CENTRE OF PROFESSIONAL RESEARCH PUBLICATIONS
ISSN 2049-3444
International Journal of Engineering and Technology Volume 7 No.3, March, 2017

Numerical Prediction of Sauter Mean Diameter from Pressure Swirl Atomizer Using Eulerian Model

S.K. Amedorme & A.A. Burluka
School of Mechanical Engineering, Institute of Thermofluids and Combustion, University of Leeds, UK

ABSTRACT

Atomizers are used in many engineering applications including spray combustion in furnaces, diesel engines, gasoline direct injection engines and gas turbine engines. Pressure swirl atomizers occupy a special position amongst other atomizers because they differ in quality of atomization, simplicity of construction, reliability of operation, low clogging and low expenditure of energy. Turbulence behaviour and the mean droplet size are indispensable considerations in the sprays and atomization process of pressure swirl atomizers. This paper presents entirely Eulerian modelling of two phase flow in a pressure swirl atomizer as a single multi-component phase with high density variations using Computational Fluid Dynamics (CFD) commercial code STAR-CD. The transport equations for the liquid surface density and liquid mass fraction are modelled for the flow and turbulent fields. Numerical results such as liquid mass fraction and liquid surface density are presented. The model also shows the results of atomization characteristics such as droplet velocity and predicts Sauter Mean Diameter (SMD) with reasonable order-of- magnitudes.

Key words: *Sauter Mean Diameter (Smd), Droplet Velocity, Eulerian Modelling, Liquid Mass Fraction, Liquid Surface Density*

NOMENCLATURE

S_m	Mass source
S_i	Momentum source
m	Mass flow rate of liquid
r_{eq}	Equilibrium drop size
P	Pressure
k	Turbulent kinetic energy
$\bar{u}$	Mean velocity
u	Velocity
$\dot{m}_{vap}$	Mean rate of vaporization
d_{32}	Sauter mean diameter
$\widetilde{Y}_{liq}$	Mass fraction of liquid
Σ	Liquid surface density
Σ_{eq}	Equilibrium interface area per unit mass
D_t	Turbulent diffusivity
Sc_{liq}	Turbulent Schmidt number
Greek symbol	
ϵ	Turbulence dissipation rate
η	Surface tension
ρ_l	Liquid density
τ_c	Turbulence time scale
$\bar{\rho}$	Average density
Subscripts and Superscripts	
l	Liquid
g	Gas
Abbreviations	
CFD	Computational Fluid Dynamics
SMD	Sauter Mean Diameter
RANS	Reynolds Averaged Navier-Stokes
LES	Large Eddy Simulation
PSA	Pressure-swirl atomizers

1. INTRODUCTION

Atomizers are used in many engineering applications including spray combustion in furnaces, diesel, direct injection petrol engines and gas turbine engines. They are also commonly used in applying agricultural chemicals to crops, paint spraying, spray drying of wet solids, food processing and cooling of nuclear cores. Atomizers are special nozzles designed to produce a rapid break-down of liquid in a two phase flow. They are used to increase the specific surface area of the fuel and thereby achieving high rate of mixing and evaporation. In most combustion systems, reduction in mean drop size leads to higher volumetric heat release rate, easier ignition, a wide burning range and lower exhaust concentrations of the pollutant emissions. Atomizers are known to affect combustion stability limits, combustion efficiency, smoke and carbon monoxide generation, and unburned hydrocarbon levels [1, 2]. The basic principle of fluid flow through the pressure swirl atomizer (PSA) is that in a swirl spray nozzle the liquid is introduced through tangential or helical passages into a swirl chamber from which it emerges through an exit orifice with tangential velocity components. As a result of the vortex flow, a hollow air core is formed, it is concentric with the nozzle axis. The outflowing thin conical liquid sheet attenuates rapidly becoming unstable and disintegrates into ligaments and then drops in the form of a well-defined hollow cone spray. In order to analyse spray and atomization characteristics in pressure swirl atomizer, computational fluid dynamics (CFD) research has been developed. Chinn et al.[3], Cooper et al. [4] and Yule and Chinn [5, 6] are pioneers in the simulation of two-phase flow in the simplex atomizers. They [6] conducted a numerical study in pressure atomizer by treating the entire computational domain as single phase and then guessing the interface by joining grid points where pressure is found to be atmospheric. Solution was re-calculated by creating a new grid using the calculated interface and treating the interface as a “with-slip” boundary. However, the condition of normal stress balance was not applied at the interface. The velocity and pressure distribution in the atomizer were calculated and discharge coefficient and spray angle were predicted. Steinthorsson and Lee [7] conducted three-dimensional simulations of internal, free-surface flow in a pressure-swirl atomizer via commercial software FLUENT. The atomizer used in the simulations is a large-scale atomizer. The Volume of Fluid (VOF) method was adopted to capture the formation of the air-core and Reynolds Stress Turbulence model was used to model the effects of turbulence. The results were compared to experimental data given by Wang et al. [8]. They concluded that the effect of the discrete inlet slots disappears before the liquid enters the orifice. Numerical simulation of laminar and turbulent two-phase flow in pressure-swirl atomizers was also carried out by Nouri-Borujerdi [9]. He coupled the laminar and turbulent Navier–Stokes equations with the explicit algebraic Reynolds stress model as well the level set model to simulate the air-water two-phase flow inside the pressure-swirl atomizer. Applying a high-order compact upwind finite difference scheme with the level set equation culminated to capture the interface between air-liquid two-phase flow and decreasing the mass conservation error in the level set equation showed that some recirculation zones were observed close to the wall in the swirl chamber and to the axis. The proposed model showed that some improvements were obtained compared with the previous numerical solutions. Hansen [10] also studied and simulated the flow in a scaled model of a Danfoss pressure-swirl atomizer through commercially available CFX-4.3 code. Two approaches were used in the simulations. A Large Eddy Simulation (LES) based on the work of Jacobsen [11] and a simulation where the flow was modelled as being laminar. The simulations were performed in a three dimensional curvilinear grid representing the swirl chamber of the atomizer and managed to capture the overall flow characteristics of a pressure-swirl atomizer with the formations of an air-core and a thin liquid film in the exit region of the swirl chamber. The results from LES and simulations assuming laminar flow were verified against experimental findings from Laser-Doppler Anemometry (LDA) and pressure measurements. Belhadef et al. [12] performed numerical studies using FLUENT to model the sprays characteristics within and outside the pressure swirl atomizer. He developed one-fluid Eulerian model to predict liquid sheet atomization with high Weber and Reynolds numbers. The model considered a single phase of liquid-gas mixture to represent the turbulent mixing of the liquid sheet with the ambient gas. As the flow was highly swirled and highly anisotropic, the Reynolds stress model was used for the turbulence. The mean liquid–gas interface density balance equation was solved to get the Sauter Mean Diameter of droplets. Recent studies show that, in Computational Fluid Dynamics (CFD), two phase flows are commonly modelled using two different approaches: The Eulerian method where the spray is considered a continuum across the whole flow domain and the Lagrangian method where the paths taken by the droplets are tracked through the domain. A combination of an Eulerian k-ε turbulence model to describe the interaction between droplets and gas phase in the secondary break-up with Lagrangian method to model the disperse phase in the secondary break-up is achieved by Lin et al.[13] and Xiong et al.[14] in a non-swirling effervescent atomisation spray. In these related works, the droplet velocity is finally calculated in the spray far field by a one- phase model initially developed for variable density jets. Within Eulerian methods, the two phase model solves state equations for each fluid and takes into account the interactions between phases. Drawbacks of this method include interfacial terms complex modelling and the high number of equations as each fluid is transported. On the other hand, entirely one-fluid Eulerian model used in this study has advantage to compute only the transport of one single fluid with high density variation [12].

2. EULERIAN MODEL

An entirely Eulerian approach proposed by Vallet et al.[15] treats a two- phase medium as a single continuum where the

dense phase is described similarly to a species in a multi-component reactive mixture.The mass and momentum conservation equations (the 'Navier-Stokes' equations) for general incompressible fluid flows in Cartesian tensor notation are shown in equations 1 and 2 respectively [16]:

$$\frac{\partial \bar{\rho}}{\partial t} + \frac{\partial}{\partial x_j}\left(\widetilde{\rho u_j}\right) = S_m \qquad 1$$

$$\frac{\partial \bar{\rho}\bar{u}_i}{\partial t} + \frac{\partial \widetilde{\rho u_j u_i}}{\partial x_j} = -\frac{\partial \bar{p}}{\partial x_i} + S_i \qquad 2$$

where t — time
x_i — Cartesian coordinate (i = 1, 2, 3)
u_i — absolute fluid velocity component in direction x_i
p — piezometric pressure $p_s - \rho_0 g_m x_m$ where p_s is static pressure, ρ_0 is reference density, the g_m are gravitational acceleration components and the x_m are coordinates relative to a datum where is defined
ρ — density
S_m — mass source
S_i — momentum source components

Let $\tilde{Y}_{liq}$ be the liquid mass fraction per unit mass of the two-phase medium, then
Conservation equation for liquid mass fraction [17]

$$\frac{\partial \bar{\rho}\,\tilde{Y}_{liq}}{\partial t} + \frac{\partial \bar{\rho}\,\tilde{u}_j \tilde{Y}_{liq}}{\partial x_j} = \frac{\partial}{\partial x_j}\bar{\rho}\frac{D_t}{Sc_{liq}}\frac{\partial \tilde{Y}_{liq}}{\partial x_j} - \dot{m}_{vap}\tilde{\rho}\tilde{\Sigma} \qquad 3$$

where $\bar{\rho}$ is the Reynold-average density, $\tilde{u}_j$ is the Favre-averaged velocity of both phases,

The mean density $\bar{\rho}$ is related to the Favre averaged liquid mass fraction $\tilde{Y}$ by

$$\frac{1}{\bar{\rho}} = \frac{\tilde{Y}_{liq}}{\rho_l} + \frac{1 - \tilde{Y}_{liq}}{\rho_g} \qquad 4$$

where ρ_l and ρ_g are the constant liquid and gas densities respectively. It is assumed that the pressure acting upon both phases is equal.
$\dot{m}_{vap}$ is the mean rate of vaporization per unit surface of the liquid $\tilde{\Sigma}$ is the mean surface area of the gas-liquid interface per unit of two-surface media. Dispersion of the liquid by the turbulence is expressed in the equation by using the turbulent diffusivity D_t and the turbulent Schmidt number as constant $Sc_{liq} = 0.7$.

Let $\tilde{\Sigma}$ be the average surface area of the liquid-gas interface per unit mass of two phase medium. The transport equation for the $\tilde{\Sigma}$ can be written as [17]

$$\frac{\partial \bar{\rho}\,\tilde{\Sigma}}{\partial t} + \frac{\partial \bar{\rho}\,\tilde{u}_j \tilde{\Sigma}}{\partial x_j} = \frac{\partial}{\partial x_j}\bar{\rho}\frac{D_t}{Sc_\Sigma}\frac{\partial \tilde{\Sigma}}{\partial x_j} + \frac{\bar{\rho}\tilde{\Sigma}}{\tau_c}\left[1 - \frac{\tilde{\Sigma}}{\Sigma_{eq}}\right] \qquad 5$$

where D_t is the turbulent diffusivity, Sc_Σ is turbulent Schmidt number and is a constant $Sc_\Sigma = Sc_t = 0.7$, τ_c is the rate of surface production and is proportional to turbulence time scale given by

$$\tau_c = C_1 \frac{\tilde{k}}{\tilde{\varepsilon}} \qquad 6$$

Σ_{eq} is equilibrium interface area and is related to equilibrium drop size r_{eq} [15, 17] by:

$$\Sigma_{eq} = \frac{3\tilde{Y}_{liq}}{\rho_l r_{eq}}, \qquad r_{eq} = C_r\left(\frac{\bar{\rho}\tilde{Y}_{liq}}{\rho_{liq}}\right)^{2/15}\frac{\eta^{2/5}}{\tilde{\varepsilon}^{2/5}\rho_{liq}{}^{3/5}} \qquad 7$$

where C_r is a constant η is the surface tension of the liquid.
The atomization model eqs.(3) and (5) require a turbulent diffusivity and an integral scale τ_c and the standard k-ε turbulence model was used to calculate these variables as well as providing closure of the fluid dynamics transport equations[18].
Once $\tilde{\Sigma}$ and $\tilde{Y}$ are calculated, the Sauter mean diameter (SMD) d_{32} and the number density n can be found as:

$$d_{32} = \frac{6\tilde{Y}_{liq}}{\rho_{liq}\tilde{\Sigma}} \qquad n = \frac{\rho_{liq}{}^2\,\tilde{\Sigma}^3}{36\pi\tilde{Y}_{liq}{}^2} \qquad 8$$

3. NUMERICAL PROCEDURE

Computations are performed thanks to the CFD commercial code STAR-CD version 4.22. The equations are solved using the finite-volume method in association with the SIMPLE and PISO algorithms and upwind differencing (UD) scheme. The SIMPLE and PISO algorithms use a relationship between velocity and pressure corrections to enforce mass conservation and to obtain velocity and pressure fields. The upwind differencing (UD) discretization is more stable and computationally less expensive. Two equations standard k-ε model has been adopted for the computation of turbulence in the fluids since there is no conclusive information available in the literature concerning accurate and suitable modification of the k-ε model for two phase flow. STAR-CD contains built-in boundary condition options that cover the majority of practical situations. The inlet (prescribed flow) which is at an inlet or 'free' boundary, where the distributions of mass flux and fluid properties are known. The outlet boundary treatment is suitable for locations where the flow is everywhere outwards-directed, but the conditions are otherwise unknown. They are, of course, mainly determined by what is happening upstream. In impermeable wall the usual no-slip prescriptions for velocity is either applied directly or, in the case of turbulent flow calculations with certain turbulence models, via 'wall functions'. These also include provision for wall roughness. Symmetry plane denotes a surface such that all field quantities on one side of it are a mirror image of those on the other side. The various boundary locations and conditions for the model are shown in Fig.1. The following quantities and values are defined as material properties for the inlet boundary regions. Liquid of density ($\rho_l = 997.5\ kg/m^3$) flows through the velocity inlet2 of 2mm diameter with air of density ($\rho_g = 1.30 kg/m^3$) passing through the other 2mm diameter inlet1 as shown in Fig.1. The inlet boundary conditions used to perform the calculations for the liquid are one (1) for liquid mass

fraction, 10% for turbulent intensity, 0.001m for turbulent length scale and 100.0 m/s for the velocity magnitude. The two air inlets conditions remain the same except for the mass fraction. The outlet boundary conditions are 1% for turbulent intensity, mass fraction of one for both liquid and air and 0.001m for the turbulent length scale. The walls represent the solid walls of the nozzle and the computational domain and standard wall functions are used to model the near-wall regions with no-slip conditions

The mesh imported into STAR-CD is shown in Fig.2. The mesh sizes were varied to determine whether the solution was grid dependent or not since it is a fact from the principle of simulation that a fine mesh produces better or accurate results and predictions than a coarse mesh though a fine grid increases the computational time. Therefore, an optimal mesh configuration is required that provides a balance between computational time and solution accuracy. It was realized after various refinements of the mesh in relation to the simulation results that a final non-uniform mesh grid composed of 83257 tetrahedral cells and 161312 faces produced better results. The distribution of the mesh was done such that the swirl chamber and the cylinder have fine and coarse meshes respectively. The refined grid spacing on the swirl chamber was about 0.15 mm and coarse mesh of 0.5 mm on the computation domain with a growth factor of 2.0. This is to reduce the computational time and for 3.20GHz Intel(R) Xeon(R) processor to accommodate. The total computational time was about six (6) hours.

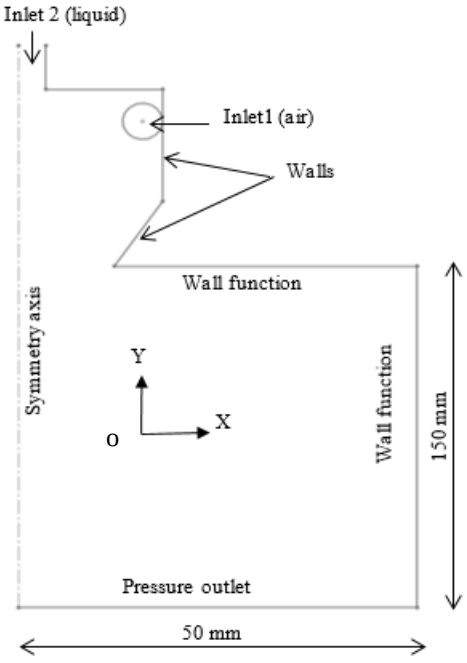

Fig. 1 The computational domain and boundary conditions

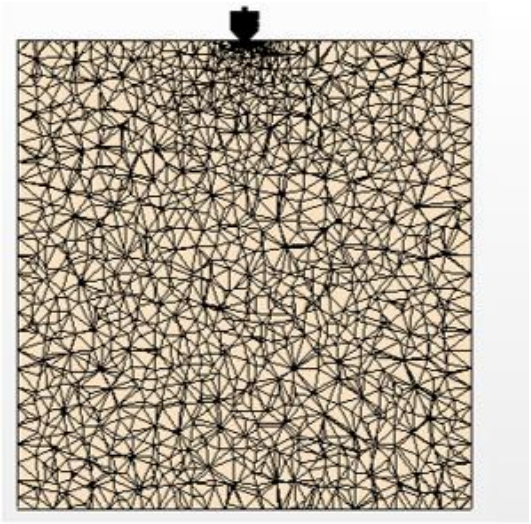

Fig.2 Mesh on vertical plane through the atomizer model

4. 3D PLOT AND SECTION PLANE

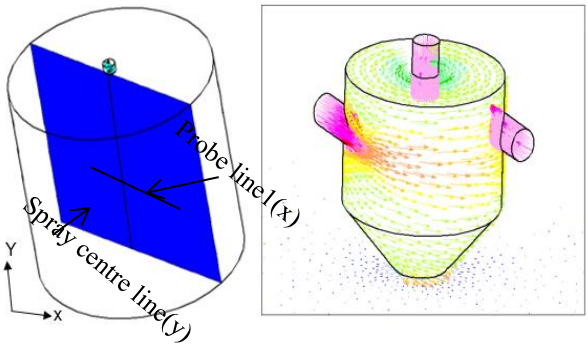

Fig. 3 Vertical section plane and 3D plot of velocity magnitude.

Fig.3 shows the vertical plane and 3D plot of the velocity magnitude. In order to have a better understanding of the flow and turbulence fields the two-dimensional vertical plane is cut through the atomizer at 180^0. The three inlets or holes are symmetrically located at the sides and the middle of the atomizer so that the spray emerging from them can be adequately captured and analysed on the plane. The nozzle exit is located at the centre of the computational domain for axisymmetric study to be carried out in the computational domain on the plane. Liquid through the middle jet and air from the other two jets are injected at a steady state and simulations were carried out using the Eulerian single-phase modelling methodology for the injected fluids with high density variation and high Weber and Reynolds numbers. This Eulerian approach treats the liquid and air as a single phase with large scale features of the flow dependent only upon density variation. Standard k-epsilon turbulence was used to model the turbulence effect. The flow simulations were carried out with the boundary condition for the air inlets taken to be a specified velocity flow rate normal to the vertical plane and liquid velocity inlet parallel to the plane. The outlet of the computational domain is set to pressure boundary. All wall boundaries are taken as no-slip. For all cases, the liquid and air were at normal

temperatures. For air and liquid respectively the densities are 1.30 and 997.5 kg/m^3. Swirl motion and directions, shown in Fig.3 indicate that the correct directions and swirling motion has been achieved**.** In order to compare the results of the flow and turbulent fields, two simulations were run for two pressure-velocity coupling algorithms (SIMPLE top and PISO bottom).

5. GRID INDEPENDENCE TEST

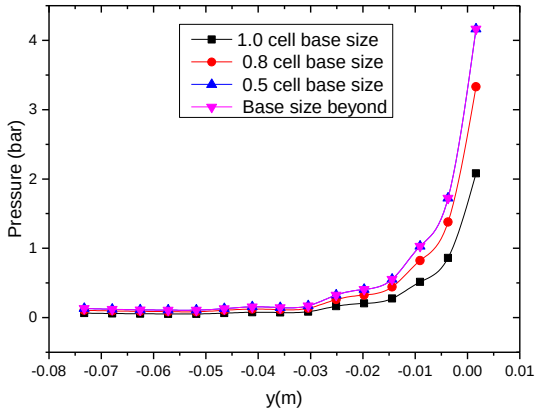

Fig. Error! No text of specified style in document. **Grid independence test using variation of pressure profile with grid sizes**

Fig. 4 presents the grid independence test using variation of pressure profile with cell sizes. The pressure variations are taken on the symmetry line shown on the vertical plane in Fig.3 and the y-axis values are the positions on the symmetry line. The black, red and blue lines represent the variation of pressure profile on the symmetry line for cells, from coarse to fine grid, with base sizes of 1.0mm, 0.8 mm and 0.5mm respectively. With simulation of cell size 1.0 mm the pressure profile has maximum value of 2.2 bars, the 0.8 mm cell size the maximum pressure profile corresponds to 3.5 bars and 4.3 bars was the maximum value for the pressure profile when the mesh base size was reduced to 0.5 mm. It was observed after carrying out this series of grid independent tests shown on Fig 4 that increasing the cells beyond 83257 cells with base size of 0.5 mm did not alter the pressure profile. Thus the numerical simulations are grid independent beyond 83257 cells of base size 0.5 mm on the symmetry line. The discretisation error for maximum pressure profile P_{max} using the Grid Convergence Index (GCI) was calculated with these relations. The relative error,e, between successive grids is found by

$$e = \frac{f_2 - f_1}{f_1}$$

where f_1 is the fine grid and f_2 is the coarse grid

For each pair of successive grids, GCI is found from

$$GCI = \frac{F_s|e|}{(r^p - 1)}$$

where $F_s = 1.25$ is the factor of safety recommended for three grid studies, r is the grid refinement ratio of 1.6, p is the order of discretisation assumed to be 2. The two errors for the three grids are shown in Table 1

Table 1 Grid statistics, pressure data and discretisation error estimates

Grid size (mm)	P_{max} (bar)	e	$GCI(\%)$
1.0	2.2	-	-
0.8	3.5	0.5909	47.30
0.5	4.3	0.2286	18.32

From Table 1 the results show that Grid Convergence Index (GCI) from coarse to fine grid is relatively low and therefore a grid independent solution is achieved.

6. FLOW AND TURBULENT FIELDS FOR SIMPLE AND PISO AlGORITHMS

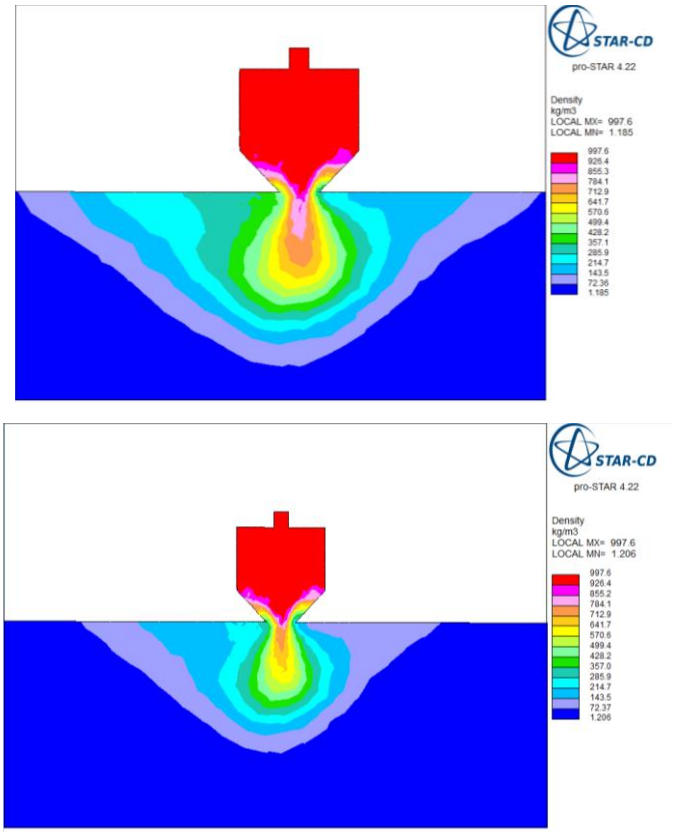

Fig. 5 Comparison of contour plot of density for SIMPLE and PISO algorithms

Fig. 5 shows the contour plot for density with 15 levels on the colour map**.** In "one-fluid-two-phase" $\Sigma - Y_{liq}$ atomization model, high mean density variation is an important parameter and depends on the Favre averaged liquid mass fraction. Flow and turbulence fields depend heavily on the mean density variation and as such to get a complete picture of the model for further analysis to be conducted density variation for the two fluids treated as a single phase fluid must first and foremost be achieved for the simulation. From the figure, the blue colour corresponds to the lowest density and the red colour representing the maximum value for the density distribution can be observed in the vicinity of the liquid entry into the atomizer. The density variation can be seen in between these two limits and is quite large in relation to the maximum and minimum values of the density distributions. This is expected

due to large density difference that exits between liquid and gases [19]. As can be seen in the spray the density variations effect is stronger upstream and becomes less extreme in the downward stream. This density variation may be due to the compressibility effects induced by high-velocity flows between the two fluids or result from the mixing of liquid and air with different densities. In this model temperatures of the liquid and gas are not considered so the density variations cannot be related to temperature variations. To know whether or not the solution has converged in order to have confidence in these results the grid independence test has been carried out. After three refinements of the mesh the result did not change and the residuals also fall within the tolerance limit. In addition, to assess whether or not these numerical results can be trusted for the density distribution, simulations were performed for two algorithms for pressure-velocity (SIMPLE and PISO) coupling. The residuals for the main parameters calculated, such as: continuity equation, momentum and turbulence model were compared for both algorithms. Under the same conditions, and low under-relaxation factors to avoid divergence of the iterations, the two algorithms showed appropriate convergence with the minimum residuals for continuity being 0.1 and 0.012 for SIMPLE and PISO respectively, and 0.0055 for momentum. With regards to computational time, the PISO case expends less CPU time than the SIMPLE case and has greater stability. The results show that the maximum local density value is 997.6kg/m^3 for both algorithms and minimum values of 1.185 kg/m^3 and 1.205 kg/m^3 for SIMPLE and PISO simulations respectively. The average density in the distributions is in the range between 499.4 and 570.5 kg/m^3. It can therefore be easily seen that there are minimal differences in the two results indicating the result for the density is good and acceptable since SIMPLE and PISO algorithms tend to produce almost the same results under the same conditions, the only difference being the procedures for coupling the pressure and velocity are different [20].

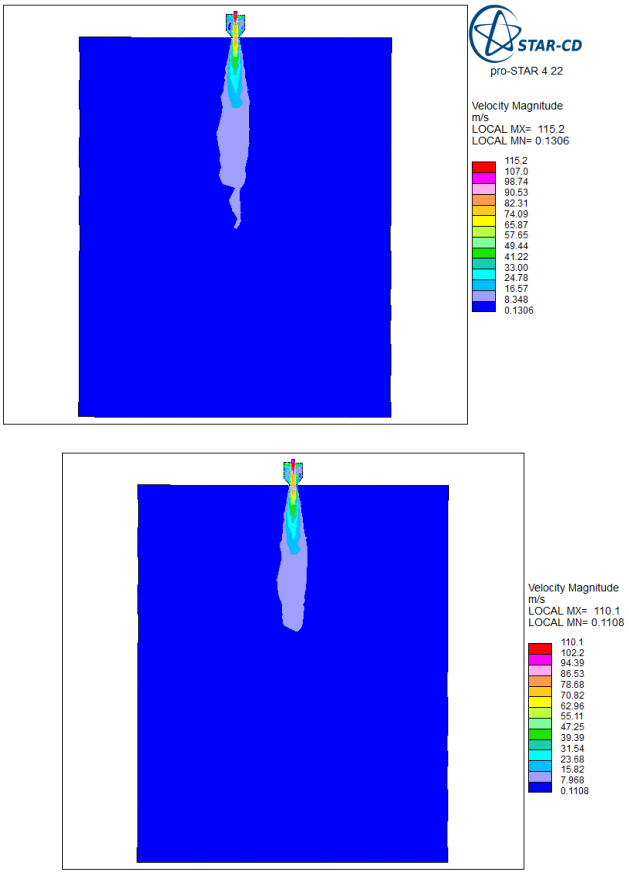

Fig. 6 Comparison of velocity magnitude contour plot on the section plane for SIMPLE and PISO algorithm

Fig.6 presents the velocity magnitude on the vertical plane for PISO and SIMPLE algorithms. The blue colour on both results represents the lowest values on the velocity distribution, which also implies that outside the spray there is only air. The minimum values of the velocity magnitude for the SIMPLE and PISO simulations are 0.013 m/s and 0.1108 m/s respectively. The red colour indicates the maximum values for the velocity on both contours and has values of 115 m/s and 110.1m/s^2 respectively. The results indicate that the average velocity in the distribution is in the range of 55.11 m/s to 55.65 m/s. The high values of the velocity in close proximity to the liquid entry into the atomizer are expected since the liquid velocity is high. The results also show that the spray is symmetrical on the vertical plane and therefor the flow behaviour can be assumed to be quasi axisymmetric. Conical spray is clearly visible and the minimum values are found downstream of the spray for both simulations. This is in conformity with the theory that liquid sheet emanating from pressure-swirl atomizer outlet widens in the form of a cone after leaving the nozzle and disintegrates downstream into droplets[21] and are mostly confined in the core regions of the spray. It can also be found that the velocity in the centre spread of the liquid is greater than the speed of the droplets at the periphery of the spray. This is especially true because at the centre axis the air will drag the smaller droplets towards the centre while the larger droplets will remain at the outer periphery and as such the velocity distribution across the plane can vary appreciably from the centre to the outer radius. The phenomena at the tip of the spray in the SIMPLE simulations may represent the break-up process

of the spray sheet into droplets which may be induced by turbulent behaviour in the spray since in turbulent flows the turbulent transport terms are dependent on the mean velocity field. It can be observed that at the same colour locations for both the SIMPLE and PISO results, the velocity field values are slightly higher for SIMPLE than PISO. These small discrepancies are acceptable since it lies within 1% and 3% as indicated by Barton [22] in his study to compare SIMPLE and PISO type algorithms for flow fields.

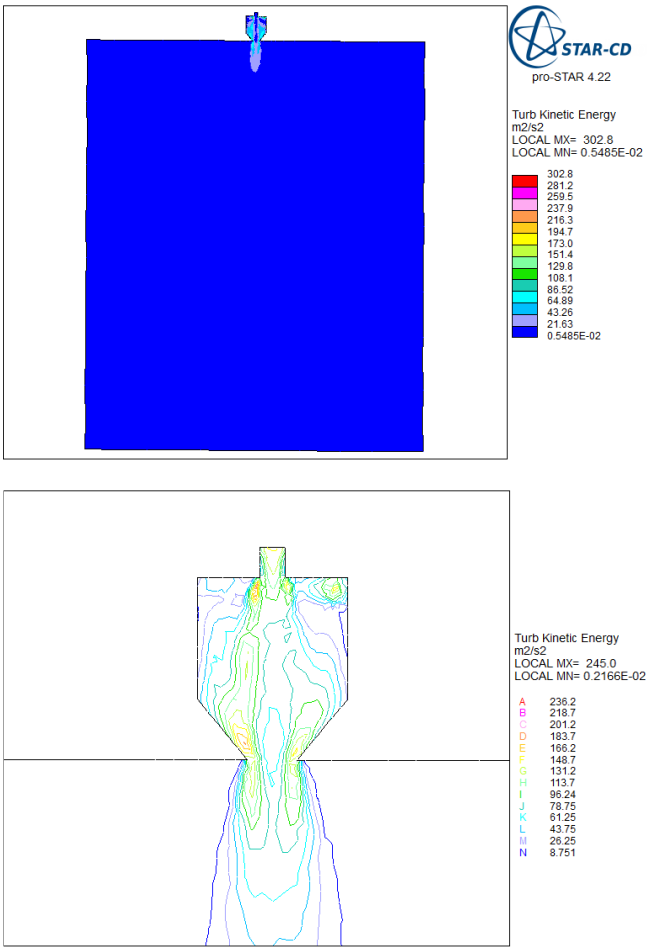

Fig.7 Comparison of turbulent kinetic energy contour plots for SIMPLE and PISO algorithm

Fig.7 shows turbulent kinetic energy on the vertical plane when the simulations for the SIMPLE and PISO algorithms were compared. The turbulent kinetic energies are colour coded such that the various colours represent localised turbulent kinetic energy at various locations in the spray. As can be seen from the two results high turbulent kinetic energy increases in the vicinity of the atomizer exit and may be due to low liquid density at those locations. It can also be observed that low turbulent kinetic energy is found in the downstream of the spray which may be due to decrease in liquid velocity and high density variation. High intensity of turbulent kinetic energy can also be seen in the liquid inlet in the PISO case and may arise from the high turbulent intensity of 10% specified at the liquid inlet. From the results turbulent kinetic energy for SIMPLE is slightly higher than the PISO results when compared at the same colour locations with the maximum turbulent kinetic energy being 302.8 m^2/s^2 and 236.2 m^2/s^2 respectively and the least turbulent kinetic energy values of $0.0055m^2/s^2$ and $0.751m^2/s^2$ respectively. The results indicate that the average turbulent kinetic energy values in the distribution corresponding to the light yellow in the SIMPLE and PISO cases are 151.4 m^2/s^2 and 148.7 m^2/s^2 respectively. The very low turbulent kinetic energy observed in the centre spread of the atomizer for the SIMPLE case may be caused by large liquid to gas ratio and may also be attributed to the inadequacies in standard k-epsilon turbulence model in predicting better turbulent kinetic energy in two phase flow. Turbulence fields depend on density variation in this atomization model [17] and as the density variation decreases greatly the standard k-epsilon turbulence model may not adequately capture this effect and might have accounted for some of these distortions or fluctuations in the turbulent kinetic energy. The fact is turbulence modelling, even for single phase flows, is an active area of research and the modelling of variable density flows particularly flows with large density ratio is certainly an unsolved problem[17].

The results also show that some recirculation zones are observed close to the walls in the swirl chamber in the PISO case and again standard k-epsilon turbulence model may not be good in predicting variable density flows which experience recirculation zones. However as stated by Beshesti et al.[17] in assessing this Σ-Y model in air-assisted atomisation, most applied numerical works are still based on this turbulence model due to its robustness and accuracy in modelling shear driven flows with minimally curved streamlines but recirculation flows are challenging for any turbulence model.

.

7. RESULT AND DISCUSSION

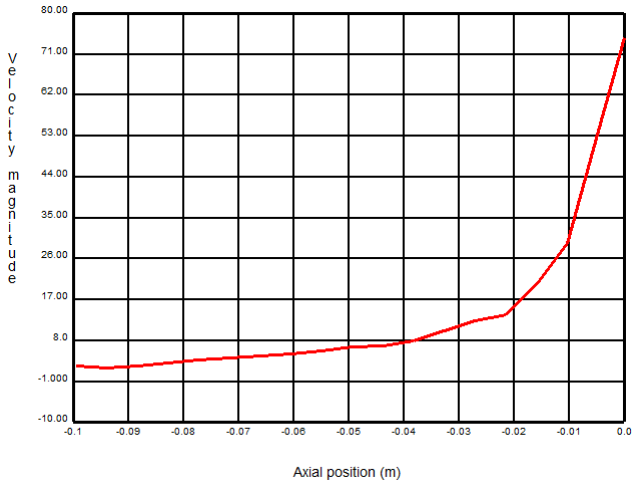

Fig. 8 Droplet velocity on the symmetry axis

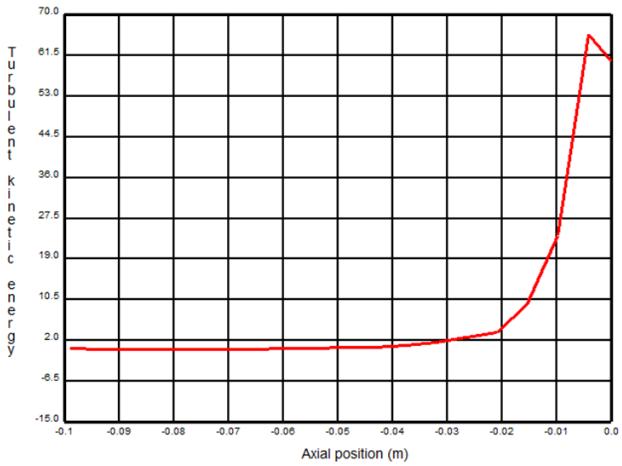

Fig. 9. Turbulent kinetic energy on the symmetry axis

Fig. 8 shows the axial profile of droplet velocity obtained on the spray axis. The values on the y-axis represent the positions on the spray centre axis from the nozzle exit to the downstream part in the computational domain. The vertical axis represents the velocity magnitude of the droplets at the various axial positions on the symmetry axis away from the nozzle exit. It can be seen that the maximum velocity at the vicinity of the nozzle exit is 74 m/s. The droplet velocity decreases quite sharply, from the nozzle exit up to 20 mm, to approximately 17 m/s. It further reduces to a low value and remain almost constant in the downstream part of the spray. Fig. 9 presents the turbulent kinetic energy on the symmetry axis. It can be observed that high turbulent kinetic energy increases in the vicinity of the atomizer exit and Low turbulent kinetic energy is found in the downstream of the spray.

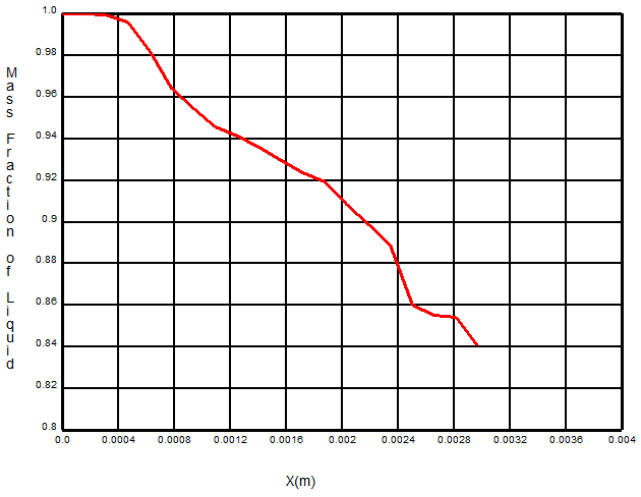

Fig.10 Mass fraction of liquid at y=5.6 mm

Fig.10 presents the graph of liquid mass fraction on the vertical plane at y = 5.6 mm. The liquid mass fraction lies between 0.7 and 1. This value implies that more liquid is injected. The liquid mass fraction is 1 at the liquid phase and 0 at the air phase. The x-axis values represent the positions as shown on the probe line 1 in Fig. 3. The liquid mass fraction on the vertical axis has a maximum value of 1. As can be seen from Fig. 10 the value of the mass fraction of the liquid is high at the centre of the atomizer at x = 0 and decreases towards the atomizer walls with the lowest value being 0.84. The high value of the liquid mass fraction at this location may be due to the initial impulse from the air emerging from the two inlets trying to reorganise with the liquid for the start of the single phase process and in attempt sandwiching the liquid in the centre spread. Liquid dispersion into the air may give rise to the decrease in the value of the liquid mass fraction. On the spray axis, the mean liquid mass fraction is almost constant with a value of 1. This is expected because the air mass fraction is zero at the liquid phase.

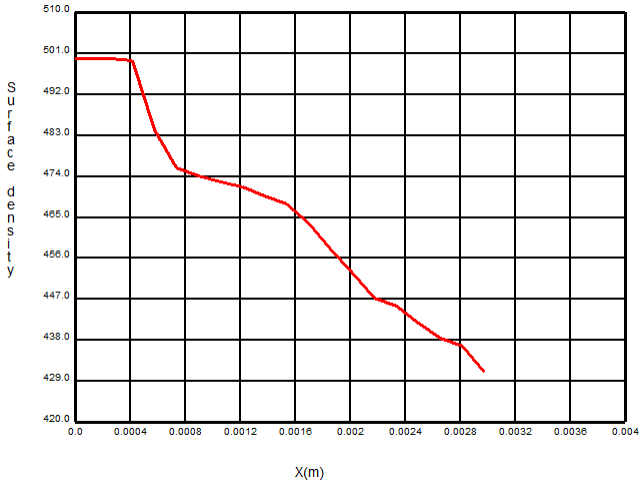

a. Predicted interfacial surface area density at y=5.9 mm

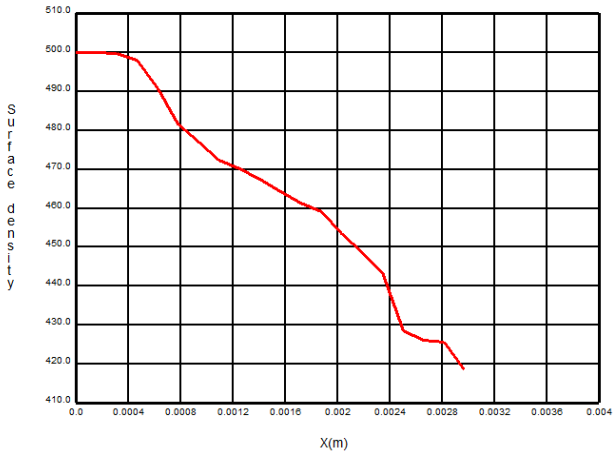

b. Predicted interfacial surface area density at y=5.6 mm

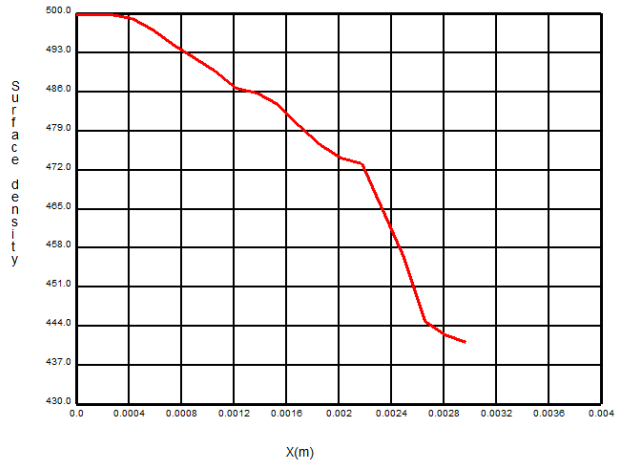

c. Predicted interfacial surface area density at y=5.2 mm

Fig.11 Predicted interfacial surface area density at y= 5.9, 5.6 and 5.2 mm

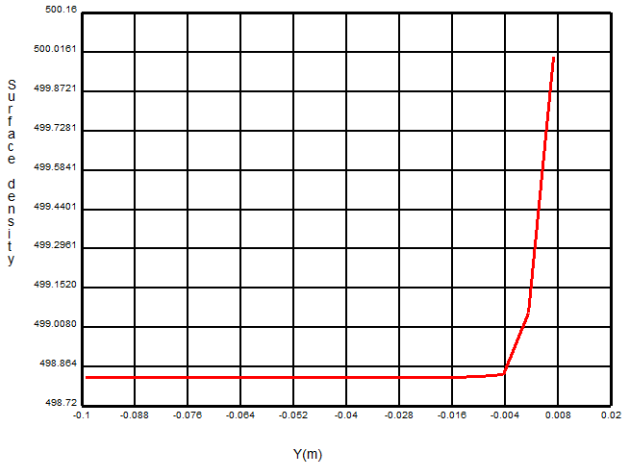

Fig.12. Predicted interfacial surface area density on the spray centre line

The liquid surface density being the key quantity characterising the atomization quality in this model is predicted across the atomizer and on the spray centre axis. Fig. 11 shows the predicted interfacial surface density at y=5.9, 5.6 and 5.2 mm. The x-axis values are taken on the distances on the probe line 1 shown in Fig. 3. The vertical axis values represent the values of the surface area density predicted on the positions on the probe line 1. The axial position x=0 corresponds to a position on the spray centre axis and extreme limit of the probe line 1. The maximum value is near the walls in the swirl chamber. These y values are located with reference to distances away from the nozzle exit in order of decreasing magnitude. The results show that the surface density has the same shape profile as the mass fraction. Minimal and maximum values of the surface density respectively are also at the point where the mass fraction values are also minimal and maximum respectively. This means that the more the liquid at a position in the field the more the surface density. In all cases of y values, the maximum value for the surface density is 500 m^{-1} at axial position x=0. This increase in the surface area density may be due to bulk turbulence of the liquid. It is supported by Besheti et al [37] that the rate of liquid surface area increase is a weighted sum of rates determined by the bulk turbulence and the drop collision.

On the predicted interfacial surface area density at y=5.9 mm the surface density remain constant between axial positions x=0 m and x=0.004 m due to more liquid mass fraction shown on Fig. 10 and reduce sharply to a value of 474.0 m^{-1} at axial position 0.0008m due to liquid dispersion and further linear decrease to a least value approximately 429.0 m^{-1} near the walls at axial position x= 0.0030 m. At the same locations for y= 5.6 the surface density is almost constant (axial positions x=0 and x=0.004 m) and also decrease to 480 m^{-1} and further reduce slightly lower than 420 m^{-1} (axial positions x=0.008 and 0.0030 m).The following are observed for the predicted interfacial surface area density at y=5.2 mm. At axial positions between x=0 m and x=0.004 m the surface density is quite high with value of 500 m^{-1} and decreases by 14 m^{-1} at position (x=0.0012 m). Near the walls the minimum value of the surface density is between 444 m^{-1} and 437 m^{-1}.

It can be deduced by comparing the liquid surface density profile at y= 5.9, 5.6 and 5.2 mm that on the spray centre axis the liquid surface is maximum and near the walls in the swirl chamber the liquid surface density is low.

Fig. 12 shows predicted interfacial surface area density on the spray centre line indicated on Fig. 3. It can be observed that the surface area density in the atomizer decrease slightly to nozzle exit (between axial position y=0 and 0.007m) from 500.0161 m^{-1} to 499.0080 m^{-1}. The coordinates (x, y = 0, 0) is located at the tip of the nozzle exit. Inside the computational domain, and on the spray centre line, the value of the predicted interfacial area density is almost constant (axial positions y = -0.004 and y = -0.1) with a value of 498.864 m^{-1} .This result is used to predict the Sauter mean diameter (SMD) on the spray axis.

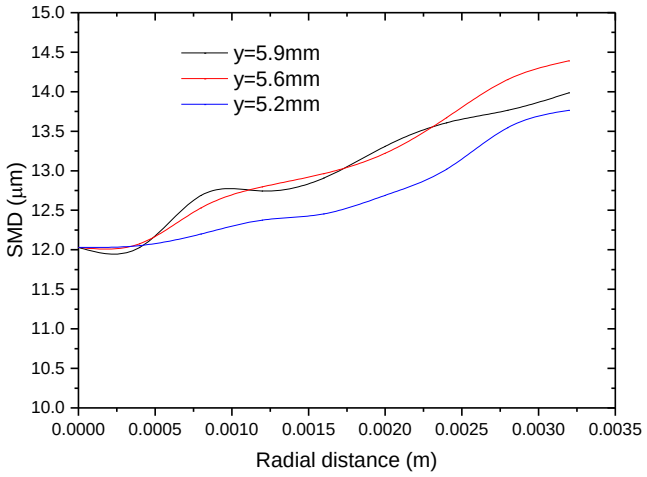

Fig.13 Sauter mean diameter (SMD) at axial positions y=5.9, 5.6 and 5.2 mm

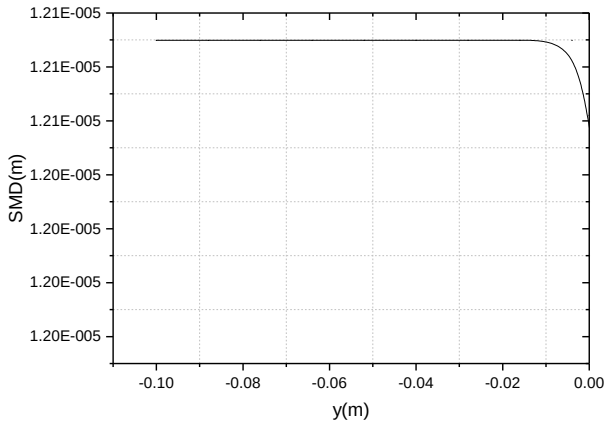

Fig.14 Spray Sauter mean diameter (SMD) predicted on the symmetry axis

Fig. 13 presents the radial profile of numerical predicted Sauter Mean diameter (SMD) at axial positions y=5.9, 5.6 and 5.2 mm from the nozzle exit. The result shows that the SMDs are smaller (12µm) in the vincity of the spray axis (axial position = 0) and a higher droplet SMD value can be seen at the periphery of the spray. Thus it can be deduced that the SMD depends on the radial distance. This may be due to the presence of large liquid mass fraction around the center axis of the spray and may also due to the large droplets experiencing less drag than the smaller droplets. Outside the liquid sheet, the mass fraction and liquid surface density are null and so the SMD calculated does not represent any droplet diameter.The result also shows that the droplet size has been predicted with correct order-of-magnitude. Fig.14 shows the Sauter mean diameter predicted on the spray axis. The y-values are the positions on the symmetry axis away from the nozzle exit in the computational domain. The curve line shows the Sauter mean diameter (SMD) predicted at the various locations on the spray centre line. The results show that the Sauter mean diameter (SMD) close to the nozzle exit is 12µm and on the other positions on the symmetry line the predicted Sauter mean diameter (SMD) is constant with a value of 12.1µm. It can be deduced that the Sauter mean diameter (SMD) increases with increasing downstream distance. This phenomenon may be attributed to droplets collisions. It can also be concluded that these Sauter mean diameter (SMD) values are predicted with correct order of magnitude and therefore can be validated.

8. CONCLUSION

In this paper, entirely one fluid Eulerian atomization model has been implemented using the STAR-CD software package. The model principally makes use of transport equation for the development of surface tension density (Σ) to characterize the rate at which surface tension energy is created. A second transport equation tracking the transport of liquid mass fraction (Y_{liq}) models the turbulent mixing of liquid. With knowledge of a local interfacial surface area and liquid mass fraction, the Sauter mean diameter is then characterized. The model predicts the droplet size (SMD) with reasonable order-of-magnitude.#

REFERENCES

Lefebvre, A., Atomization and sprays. Vol. 1040. 1989: CRC press.

Lefebvre, A.H. and D. Hallal, Gas Turbine Alternative Fuels and Emissions. CRC, Boca Raton, FL, 2010.

Chinn, J., A.J. Yule, and H. De Keukelaere. Swirl Atomizer Internal Flow: A Computational and Experimental Study. in 12th Annual Conference of ILASS-Europe, Lund, Sweden. 1996.

Cooper, D., A. Yule, and J. Chinn. Experimental measurements and computational predictions of the internal flow field in a pressure swirl atomizer. in Proc. ILASS-Europe. 1999.

Yule, A. and J. Chinn, The internal flow and exit conditions of pressure swirl atomizers. Atomization and Sprays, 2000. **10**(2): p. 121-146.

Yule, A. and J. Chinn. Pressure swirl atomizer internal flow and performance. in Proceedings of the 10th annual conference on liquid atomization and spray systems ILASS, Americas. 1997.

Steinthorsson, E. and D. Lee. Numerical simulations of internal flow in a simplex atomizer. in ICLASS-2000. 2000.

Wang, D., et al. Experimental study on large-scale simplex nozzle. in the 35th AIAA/ASME/SAE/ASEE Joint Propulsion Conference and Exhibit. 1999.

Nouri-Borujerdi, A. and A. Kebriaee, Numerical simulation of laminar and turbulent two-phase flow in pressure-swirl atomizers. AIAA journal, 2012. **50**(10): p. 2091-2101.

Hansen, K., et al., A computational and experimental study of the internal flow in a scaled pressure-swirl atomizer. Zaragoza, 2002. **9**: p. 11.

Jacobsen, C.B., Large eddy simulation of confined swirling flow: a numerical and experimental investigation of isothermal combustion chamber flows. 1997: unknown.

Belhadef, A., et al., Pressure-swirl atomization: Modeling and experimental approaches. International Journal of Multiphase Flow, 2012. **39**: p. 13-20.

Lin, J., et al., Effects of operating conditions on droplet deposition onto surface of atomization impinging spray. Surface and Coatings Technology, 2009. **203**(12): p. 1733-1740.

Xiong, H.-B., J. Lin, and Z.-F. Zhu, Three-dimensional simulation of effervescent atomization spray. Atomization and Sprays, 2009. **19**(1).

Vallet, A., Burluka, AA and R. Borghi, Development of a Eulerian model for the "atomization" of a liquid jet. Atomization and sprays, 2001. **11**(6).

Guide, Star-CD., Version 4.16. CD-Adapco, London, 2011.

Beheshti, N., A.A. Burluka, and M. Fairweather, Assessment of Σ− Y liq model predictions for air-assisted atomisation.

Theoretical and Computational Fluid Dynamics, 2007. **21**(5): p. 381-397.

Beheshti, N., A. Burluka, and M. Fairweather. Atomisation In Turbulent Flows: Modelling For Application. In Tsfp Digital Library Online. 2003. Begel House Inc.

Demoulin, F.-X., et al., A new model for turbulent flows with large density fluctuations: application to liquid atomization. Atomization and Sprays, 2007. **17**(4).

Versteeg, H.K. and W. Malalasekera, An introduction to computational fluid dynamics: the finite volume method. 2007: Pearson Education.

Nonnenmacher, S. and M. Piesche, Design of hollow cone pressure swirl nozzles to atomize Newtonian fluids. Chemical Engineering Science, 2000. **55**(19): p. 4339-4348.

Barton, I., Comparison of SIMPLE-and PISO-type algorithms for transient flows. International Journal for numerical methods in fluids, 1998. **26**(4): p. 459-483.

